A ROBUST *K* ESTIMATION SCHEME USING MESH-INSENSITIVE STRUCTURAL STRESSES

P. Dong, J.K. Hong, Z. Cao
Center For Welded Structures Research, Battelle (USA)
E-mail: dongp@battelle.org

ABSTRACT

In this paper, the applications of a new structural stress method, referred as a mesh-insensitive structural stress method developed recently, in estimating stress intensity factors for welded joints will be discussed. The new structural stress method is based on the considerations of separating an actual stress state into two parts: (1) equilibrium-equivalent part and (2) self-equilibrating part. Both parts are consistent with the far-field stress state with respect to a hypothetical crack location within fracture mechanics context. Therefore, the stress intensity factors (*K*) can be estimated once the mesh-insensitive structural stresses become available. The method is particularly suited for applications in welded joints in complex structures. In this paper, a brief description of the mesh-insensitive structural stress procedure is reviewed. A robust *K* estimation procedure is then presented. The new *K* solution procedures were then validated against a series of well-known *K* solutions for welded joints in the literature. Finally, discussions are given in terms of the implications of the present solutions in applications in complex structures.

IIW-Thesaurus keywords: *Welded joints; Stress analysis; Finite element analysis; Computation; Structural analysis; K1C; Stress; Stress distribution; Notches; Notch effect; Fracture mechanics; Crack pattern; Cracking; Defects; Influencing factors; Test pieces; Comparisons; Evaluation; Reference lists.*

1 INTRODUCTION

In performing fracture and fatigue evaluation for welded structures, stress intensity factor solutions are needed by considering crack-like discontinuities at welds. Although finite element methods can be used through either a *J* integral approach and or a direct *K* calculation using either stresses or displacements, the computational procedures involving crack tip element definitions can be too complicated to be practical. Weight function methods only require the stress distributions to be known in uncracked bodies and therefore are more attractive for practical applications. However, in using weight function approach, consistent normal stress determinations with respect to a hypothetical crack plane in finite element models are not an easy task since sharp notches at the welds introduce mesh-dependency in stress values calculated using finite element models [1-3]. Often, a fictitious notch radius had to be introduced in the finite element model to eliminate such stress singularity [1-2]. In addition to uncertainties in calculated stresses, element refinements in the order of the assumed notch radius must be used [1-2], which severely limits these calculations to only simple joint geometries.

Recently, a mesh-insensitive structural stress method has been developed by Dong and co-workers [3-6]. The underlying principle in the mesh-insensitive structural stress method is based on equilibrium considerations in displacement based finite element theory. The structural stress parameter so calculated becomes the statically equivalent far-field stresses with respect to a hypothetical crack location, but without modelling actual crack. The equivalence to the far-field stress definition in fracture mechanics enables a direct calculation of the corresponding stress intensity factors by using an existing reference *K* solution [3] for simple fracture specimen geometry. Due to the mesh-insensitive nature of the structural stress calculations, the method is particularly effective for applications in fracture and fatigue evaluation of complex structures.

In this paper, we start a brief introduction of the mesh-insensitive structural stress method and corresponding notch stress estimation procedure [3-6] for arbitrary weld geometry. The stress intensity solutions not only provide consistent stress intensity estimations for crack sizes being infinitesimally small at notch roots, but also recover accurately the stress intensity factors for long cracks that are controlled by the equilibrium equivalent far-field stresses. The validity of the new stress intensity solutions are validated by the existing weight function based solutions.

2 NEW NOTCH STRESS ANALYSIS PROCEDURES

With a new definition of structural stress concept, Dong and his co-workers [3-6] have developed a series of

Doc. IIW-1644-03 (ex-doc. X-1548-03) recommended by publication by Commission X “Structural performances of welded joints – Fracture avoidance”

mesh-insensitive stress calculation procedures for calculating the equilibrium-equivalent structural stress as shown in Fig. 1 (b) and estimating the self-equilibrium notch stresses as shown in Fig. 1 (c) in sharp notched components. Their applications in fatigue evaluation and fracture analysis of welded joints have been given in a series of recent publications [3-6]. In what follows, the mesh-insensitive structural stress procedure is briefly highlighted, particularly for estimating stresses and stress intensities at notches. Additional details can be found in the above cited publications. The structural stress definition that follows elementary structural mechanics theory can be established with following considerations:

It can be postulated that for a given local through-thickness distribution as shown in Fig. 1 (a) obtained from a finite element model, there exists an equilibrium-equivalent structural stress distribution normal to a hypothetical crack plane from a notch, as shown in Fig. 1 (b), in the form of membrane and bending components. Note that in fracture mechanics context, such a structural stress definition becomes the equivalent far-field stress (σ^{∞}) definition. While local stresses near a notch are mesh-size sensitive due to the asymptotic singularity behaviour as a notch tip is approached, the imposition of the equilibrium conditions in the context of elementary structural mechanics within a reference region should eliminate or minimise the mesh-size sensitivity in the structural stress calculations. Within the context of displacement based finite element methods, the most accurate solution variables are nodal displacements and balanced nodal forces (or internal forces at an element level) at nodal positions before stresses and strain were computed, on which equilibrium conditions are directly enforced. Therefore, the nodal displacements and nodal forces can be directly used to extract the far-field stress at a notch. This method is particularly convenient for characterising stress states at notch in shell/plate type structures where shell/plate element models are typically used. The detailed procedures are given by Dong *et al.* [3-6], along with a series of numerical examples to demonstrate that essentially the same stresses were obtained at the notch root with drastically different element sizes and element types at both specimen and structural levels.

2.1 Characterisation of far-field stresses

Most of the crack growth data has been generated from standard fracture mechanics specimens with a notch as a crack starter. Most of these specimens can be conveniently modelled as either 2D or simple 3D solid specimens in the finite element context. The new stress analysis procedures can be implemented by using stress quantities from a solid element model as follows (although balanced nodal forces are more robust when using coarse finite element models [3]).

As shown in Fig. 2, a typical through-thickness stress distribution at a notch root typically exhibits a monotonic through-thickness distribution with the peak stress occurring at the root of notch. It should be noted that in typical finite element based stress analysis, the stress

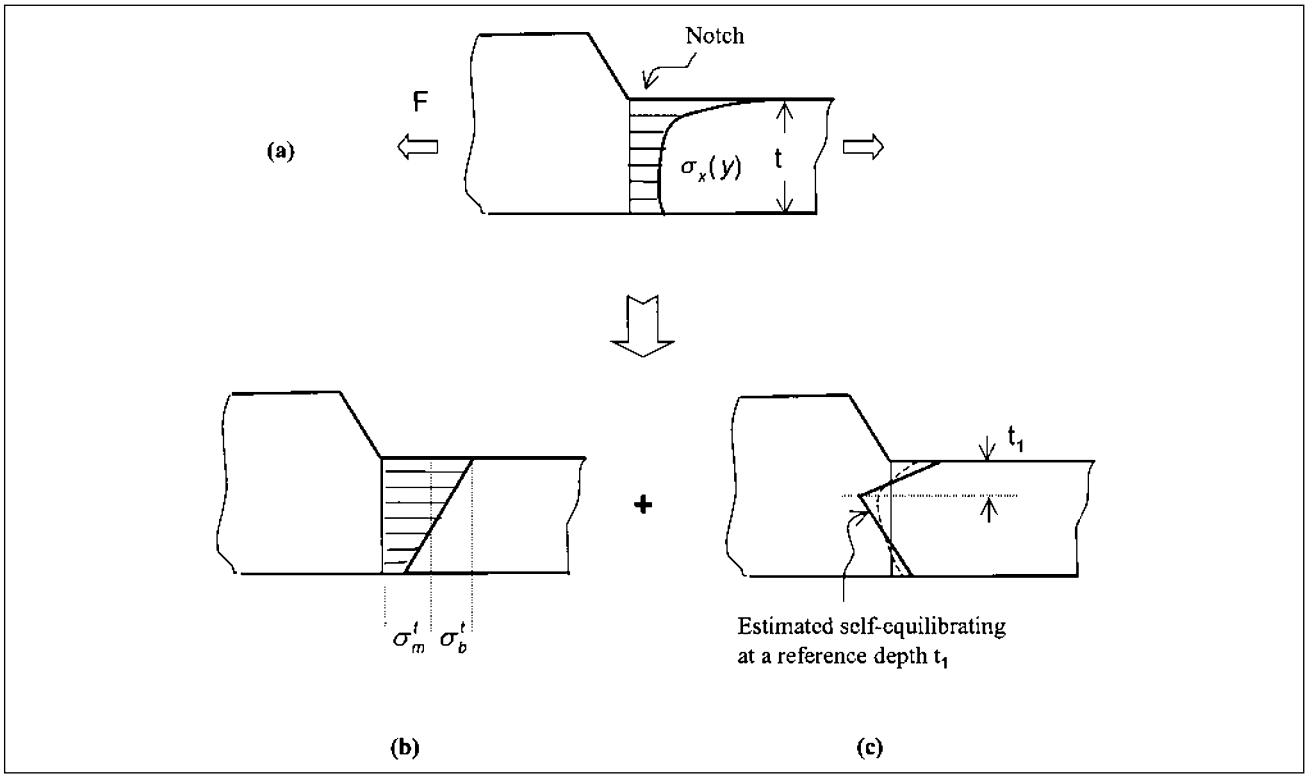

Fig. 1. Through-thickness structural stresses definition.
(a) Local stresses from FE model at a notch.
(b) Equilibrium-equivalent structural stress or far-field stress.
(c) Approximation of self-equilibrating stress (notch stress) with respect to a reference depth t_1

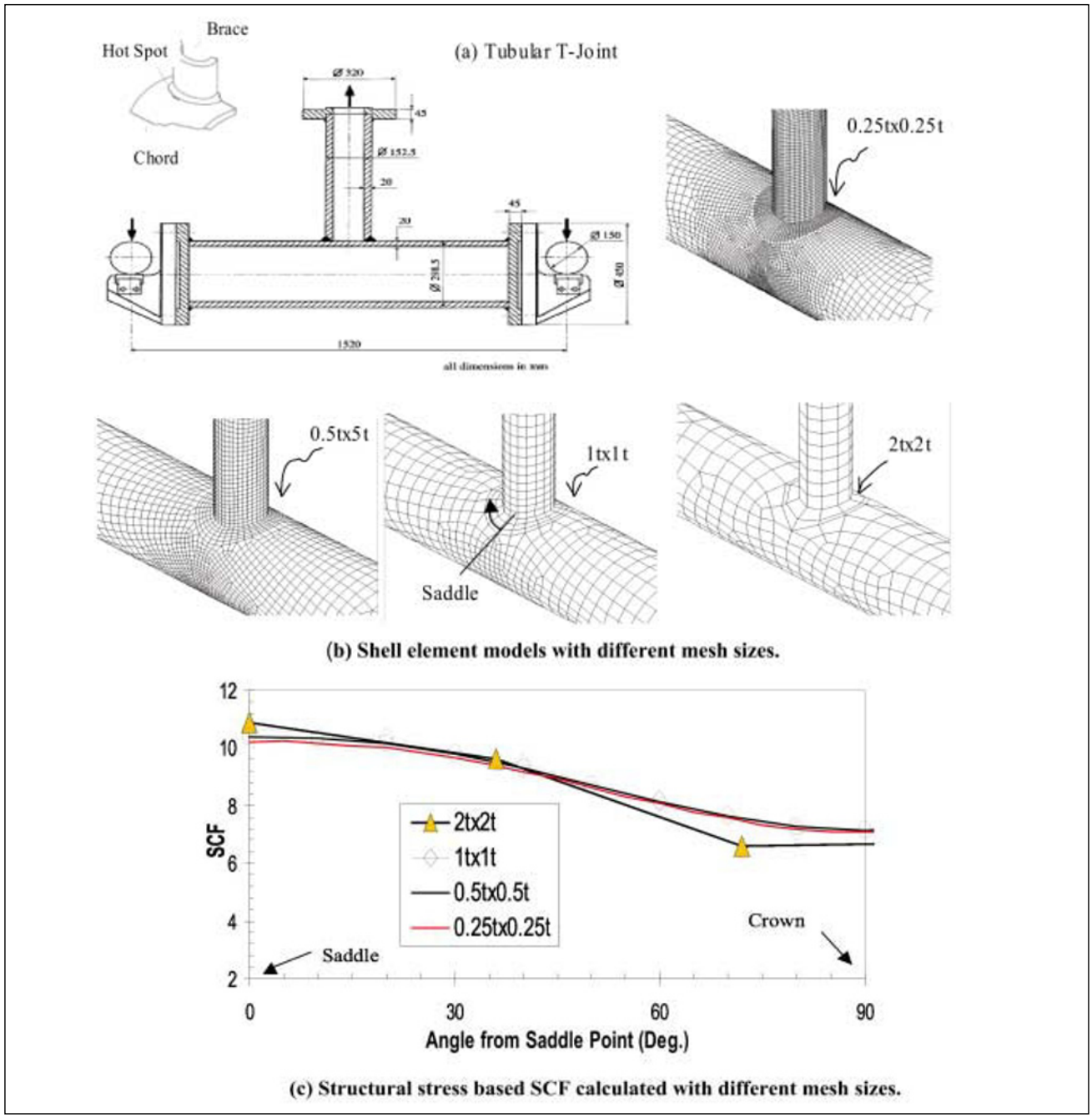

Fig. 2. Mesh-insensitivity demonstration for equivalent far-field stresses along tube to tube joint.
(a) A tubular joint from [8].
(b) Four FE shell models with various element sizes at the weld.
(c) Comparison of calculated far-field stresses at the weld toe (without modelling the presence of the weld) from the four models.

values within some distance from the notch root can change significantly as different element sizes or element types are used in a finite element model [16-19], referred to as mesh-size sensitivity in those publications. The corresponding statically equivalent structural stress distribution is illustrated in Fig. 1 (b), in the form of a membrane component (σ_m^t) and bending component (σ_b^t), consistent with elementary structural mechanics definition:

$$\sigma_s^t + \sigma_m^t + \sigma_b^t \tag{1}$$

The super script t signifies the definition of the structural stress is with respect to ligament length t in Fig. 1(a) from the notch root.

In a series of recent publications [3-7], the use of 3D solid element models by enforcing equilibrium conditions to achieve a relative mesh-insensitivity were discussed in [3-6]. In practical applications, the mesh-insensitive structural stress methods can be most effectively implemented for shell or plate element models for arbitrarily curve welds as discussed in [5-7] by solving a system of simultaneous equations using balanced nodal forces and moments from typical finite element solutions. A tubular joint example was discussed in detail in Dong and Hong [7] recently and summarised in Fig. 2 for demonstrating the effectiveness of the mesh-insensitive structural stress procedures. Some of the considerations can also be inferred from this example. As seen

in Fig. 3, once an element size of about $2t \times 2t$ (here, t is the tube thickness) in using linear elements, the curved surface around the tube to tube intersections can no longer be corrected modelled in this example. As a result, the structural stress based SCF around weld starts to lose accuracy.

2.2 Fracture mechanics applications

The far-field or far structural stress parameter calculated as discussed in the previous section has a direct relevance to fracture mechanics applications. As shown in Fig. 3, $\sigma^{\infty}(x)$ represents the statically equivalent far-field stress with respect to a hypothetical crack plane in fracture mechanics definition. The mesh-insensitive structural stress procedure transforms the stress state at a location of interest at a joint in complex structures under an arbitrary loading to a simple 2D crack problem subjected to an equivalent far-field stress state. This far-field stress distribution is fully described by Eq. (1) as the membrane plus bending, for instance:

$$\sigma^{\infty}(x) = \sigma_s^t - \frac{2\sigma_b^t x}{t} \tag{2}$$

which can directly enter K solution equations for a crack in a smooth plate such as an edge crack situation as shown in Fig. 3. The detailed K formulation using the mesh-insensitive structural stresses will be given in the next section after presenting the notch stress estimation scheme. The equivalence between the far-field stress and the mesh-insensitive structural stress has been established in the previous section in view of the fact that the both definitions are solely based on statically equivalent requirements under external loads. As a special case, if a structure or component is loaded under statically determinant conditions, both the structural stress and far-field stress becomes a nominal stress, provided that nominal stress can be calculated using simple structural mechanics theory. For general non-linear far-field stress distribution $\sigma^{\infty}(x)$, well-known weight function methods can be used for calculating K as follows, e.g., for mode I crack in Fig. 3:

$$K = \int_0^a \sigma^{\infty}(x)\, w\,(x, a)\, da \tag{3}$$

where $w(x,a)$ is weight function depending upon joint geometry [1-2] and are only available for a few simple joint types.

2.3 Characterisation of self-equilibrating stress state

As illustrated in Fig. 1, the stress distribution along the ligament (t) at the notch root can be represented by two simple stress states: an equilibrium-equivalent far-field stress state (Fig. 1 (b)) and a notch stress state that equilibrates within itself along ligament t (dashed lines Fig. 1 (c)). Before constructing analytical-based solution for the self-equilibrating notch stress distribution, an effective mean of quantifying the self-equilibrating part of the stress distributions from finite element models must be established, without relying on the direct subtraction from the FE results (dashed lines in Fig. 1 (c)) by that in Fig. 1 (b). Otherwise, infinitesimally small elements in a FE model would be required for the results to be meaningful at the notch.

By taking advantage of the mesh-insensitive procedures presented in the above for calculating equivalent far-field stresses, the self-equilibrating part of the stress state (dashed lines) can be estimated, in the equilibrium sense, by introducing a bilinear distribution with a characteristic depth t_1. Both the justification and selection of t_1 will be discussed in detail in the later sections. For the time being, in all calculations t_1/t is taken as 0.1. The stress distribution representing the self-equilibrating part of the stress distributions can be considered as two

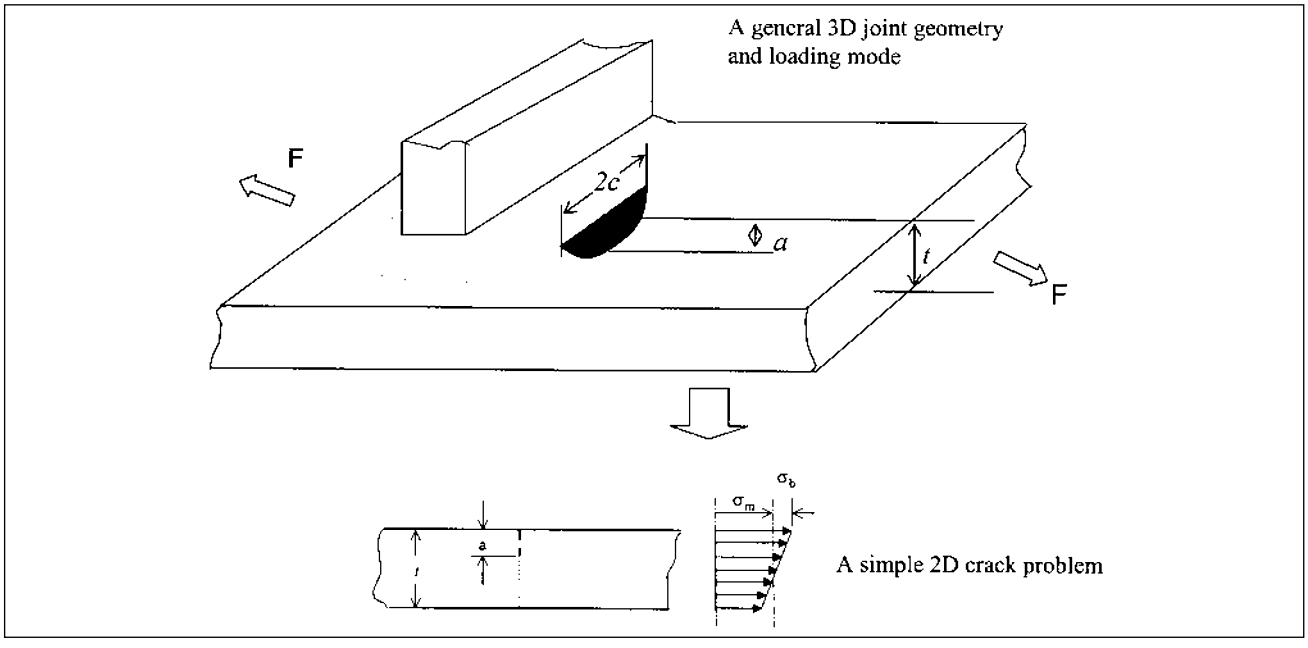

Fig. 3. Structural stress based transformation from complex 3D geometry and load mode to a simple 2D crack problem.

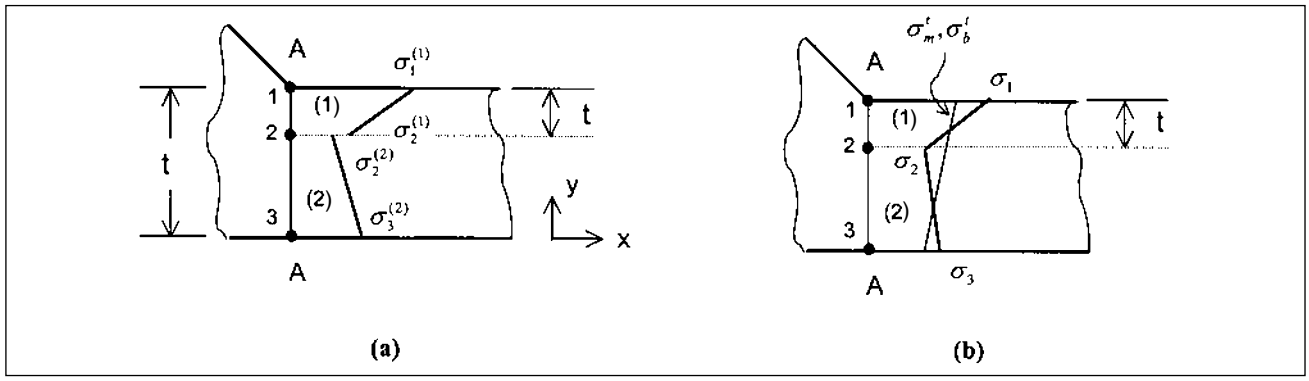

Fig. 4. Estimation of self-equilibrating part of the stress state induced by notch.
(a) After applying Eqs. (4) and (5).
(b) Imposing equilibrium requirements for regions (1) and (2) and continuity at location 2.

linear distributions within Regions (1) and (2), respectively, as shown in Fig. 4 (a). By using balanced nodal forces in a solid element model (e.g., 2D model in the present case), the normal stresses $\sigma_1^{(1)}$, $\sigma_2^{(1)}$, $\sigma_2^{(2)}$ can be calculated. By enforcing equilibrium conditions and traction continuity at Position 2, as shown in Fig. 4 (b), the following equations are obtained:

$$\begin{aligned} &2\sigma_1^{(1)} + \sigma_2^{(1)} = 2\sigma_1 + \sigma_2 \\ &t_1(2\sigma_2^{(1)} + \sigma_1^{(1)}) + (t - t_1)(2\sigma_2^{(2)} + \sigma_3^{(2)}) = \\ &t_1(2\sigma_2 + \sigma_1) + (t - t_1)(2\sigma_2 + \sigma_3) \\ &2\sigma_3^{(2)} + \sigma_2^{(2)} = 2\sigma_3 + \sigma_2 \end{aligned} \quad (4)$$

In the above equations, the unknowns σ_1, σ_2, and σ_3 at the three positions can be readily solved, resulting:

$$\begin{aligned} \sigma_1 &= \frac{1}{2}\cdot(2\cdot\sigma_1^{(1)} + \sigma_2^{(1)} - \sigma_2^{(2)}) - \frac{t_1}{2\cdot t}\cdot(\sigma_2^{(1)} - \sigma_2^{(2)}) \\ \sigma_2 &= \sigma_2^{(2)} + \frac{t_1}{t}\cdot(\sigma_2^{(1)} - \sigma_2^{(2)}) \\ \sigma_3 &= \sigma_3^{(2)} + \frac{t_1}{2\cdot t}\cdot(\sigma_2^{(2)} - \sigma_2^{(1)}) \end{aligned} \quad (5)$$

Note that within Regions (1) and (2), the equivalent membrane and bending components:

$$\sigma_m = \frac{\sigma_1 + \sigma_2}{2},\ \sigma_b = \frac{\sigma_1 - \sigma_2}{2},\ \sigma'_m = \frac{\sigma_2 + \sigma_3}{2},\ \text{and}\ \sigma'_b = \frac{\sigma_2 - \sigma_3}{2}, \quad (6)$$

respectively. The expressions in Eq. (6) fully describe the self-equilibrating part of the stress state as described in Fig. 1 (c) at a reference depth t_1. The overall far-field stress (σ_m^t and σ_b^t) corresponding to the notch ligament t can be directly calculated by using shell element procedures as described in [6-7] and illustrated in Fig. 2.

2.4 Notch stress estimation

To relate the notch stress estimation to stress intensity factor solutions, an equivalent crack face pressure (or traction without a crack) for an arbitrarily small crack is all required in view of superposition principles. To achieve this, it is assumed that the notch-induced self-equilibrating stress distributions can be estimated in terms of equilibrium-equivalent tractions within an arbitrary reference depth of l as shown in Fig. 5 in terms of p_m and p_b in Fig. 5. This can be accomplished by successively re-distributing the intersecting areas between the distributions described by σ_m^t and σ_b^t and σ_m and σ_b, as illustrated in Fig. 5 for any given l. In doing so, the self-equilibrating conditions for the notch stress distribution is maintained. The detailed discussions on solving four equations and four unknowns are given [2]. As shown by Dong *et al.* [3], a simplified solution without losing any noticeable accuracy can be obtained by assuming $p_m' - p_b' = \sigma_m' - \sigma_b'$ in Fig. 5. As a result, the following expressions are obtained, with l varying from $0 < l/t \le 1$:

$$\begin{aligned} P_m &= a_1\sigma'_m + b_1\sigma'_b + c_1\sigma^t_m + d_1\sigma^t_b \\ P_b &= a_2\sigma'_m + b_2\sigma'_b + c_2\sigma^t_m + d_2\sigma^t_b \\ P'_m &= a_3\sigma'_m + b_3\sigma'_b + c_3\sigma^t_m + d_3\sigma^t_b \\ P'_b &= a_4\sigma'_m + b_4\sigma'_b + c_4\sigma^t_m + d_4\sigma^t_b \end{aligned} \quad (7)$$

where, for instance, the coefficients a_1, a_2, a_3, a_4 in the above are expressed as:

$$a_1 = \frac{t^2 - 3lt + 2l^2}{2tl},\ a_2 = \frac{t^2 + lt - 2l^2}{2tl} \quad (8)$$

$$a_3 = \frac{-t + 2l}{2t},\ a_4 = -\frac{3t - 2l}{2t}$$

It is important to note that the above equations are valid for $0 < l/t \le 1$, recovering the solution corresponding to those described by σ_m, σ_b, σ_m' and σ_b' and σ_b' at $l/t = t_1/t$ and that described by σ_m^t and σ_b^t at $l/t = 1$.

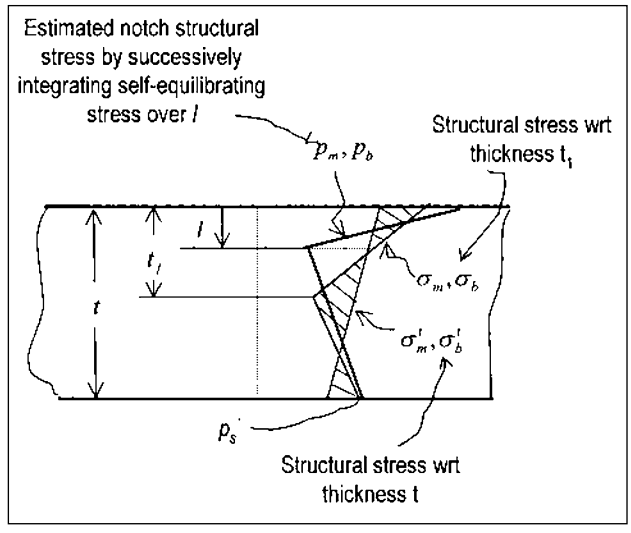

Fig. 5. An estimation scheme for equivalent crack face pressure for a hypothetical crack with at an arbitrary depth (*l*) from the notch root.

With the above notch stress estimation procedures, the normal tractions in terms of p_m and p_b along the vertical line emanating from the notch root are shown in Fig. 6 for a notch specimen taken from [1-2]. Note that the tractions in terms of p_m and p_b here should not be interpreted as local stresses. They should be interpreted as equivalent crack face tractions measured in terms of both membrane and bending within a reference depth *l*, but without the presence of a crack.

3 STRESS INTENSITY FACTOR ESTIMATION

As discussed in Dong *et al.* [3-6], the present stress analysis procedures serve as an effective stress transformation process from complex geometry (with a notch) and loading mode to a simple specimen geometry (see Fig. 3) upon which both the far-field and notch stresses act. For the simple specimen geometry, reference stress intensity factor solutions in terms of σ_m^t and σ_b^t are readily available in the open literature, e.g. the handbook by Tada *et al.* [21].

3.1 Stress intensities due to far-field stresses

Edge Cracks

In [3-6], it was shown that the Mode I stress intensity factor can be expressed as (using superposition principles) for edge cracks [9]:

$$K = K_m + K_b = \sqrt{t}\left[\sigma_m^t f_m\left(\frac{a}{t}\right) + \sigma_b^t f_b\left(\frac{a}{t}\right)\right] \tag{9}$$

The $f_m(a/t)$ and $f_b(a/t)$ are dimensionless functions of relative crack size *a/t* for the membrane and bending components of the far-field stress state, given as [9]:

$$f_m\left(\frac{a}{t}\right) = \left[0.752 + 2.02\left(\frac{a}{t}\right) + 0.37\left(1 - \sin\frac{\pi a}{2t}\right)^3\right]\frac{\sqrt{2\tan\frac{\pi a}{2t}}}{\cos\frac{\pi a}{2t}}$$

$$f_b\left(\frac{a}{t}\right) = \left[0.923 + 0.199\left(1 - \sin\frac{\pi a}{2t}\right)^4\right]\frac{\sqrt{2\tan\frac{\pi a}{2t}}}{\cos\frac{\pi a}{2t}}$$

As discussed earlier, σ_m^t and σ_b^t signify far-field structural stress components that are defined with respect to the entire thickness (*t*), as illustrated in Fig. 5. Once the structural stresses are available, the stress intensity factor can be readily calculated from the above equations.

Elliptical Cracks

Under the given far-field stress components (σ_m^t, σ_b^t), the corresponding elliptical crack solutions can be constructed in the same way as for the edge cracks in the above. The reference K solution can be taken directly from Shiratori *et al.* [10] or other reference solutions in the literature. In adopting the elliptical crack K solutions for a plate from [10], the remote stress definitions used in [10] (simple tension σ_0^m and simple bending σ_0^b) can be related to the present definitions of far-field stresses as:

$$\sigma_0^b = \frac{2a}{t}\sigma_b^t$$

$$\sigma_0^m = \sigma_m^t + \sigma_b^t - \frac{2a}{t}\sigma_b^t$$

Then, stress intensity factor solution for an elliptical crack at the deepest position (*a*) is given below:

$$K_n = \sigma_s^t\sqrt{t}\sqrt{\frac{\pi\frac{a}{t}}{Q}}\left[Y_0 - 2R\frac{a}{t}\cdot(Y_0 - Y_1)\right] \tag{10}$$

where $\sigma_s^t = \sigma_m^t + \sigma_b^t$, and $R = \sigma_b^t / \sigma_s^t$. The dimensionless parameters *Q*, Y_0, and Y_1 are documented in [22] based on a large number of parametric finite element analyses.

3.2 Stress intensities including notch effects

As discussed in Section 2, the notch stress distributions can be characterised as equivalent tractions at a hypothetic crack face (Fig. 5) and described by Eq. (8). By setting *a = l* and re-arranging Eq. (10) for edge cracks, the Mode I stress intensity factor including the estimated notch effects is expressed as, for any given crack size *a*:

$$K = \sqrt{t}\,p_s\left[f_m - r\frac{t}{a}(f_m - f_b)\right] \tag{11}$$

where $p_s = p_m + p_b$ and $r = p_b / p_s$ as illustrated in Fig. 5. For an elliptical crack, the notch stress intensity factor from Eq. (10) becomes:

$$K = p_s\sqrt{t}\sqrt{\frac{\pi\frac{a}{t}}{Q}}\left[Y_0 - 2r(Y_0 - Y_1)\right] \tag{12}$$

where p_m and p_b are given by the expressions in Eq. 8.

3.3 Validations

The weight function based stress intensity solutions by Glinka and co-workers [1-2] are used here as a valida-

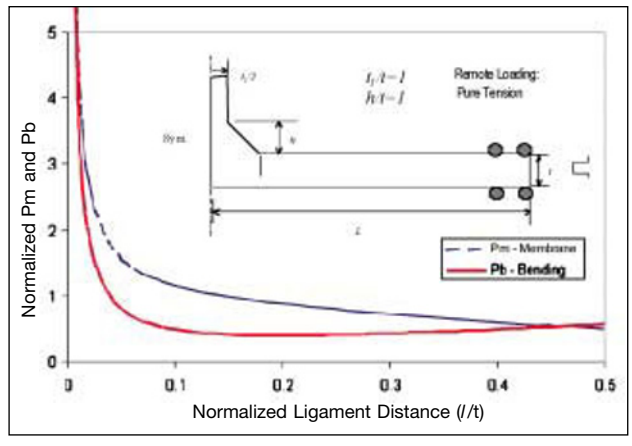

Fig. 6. Notch stress estimation – Linear tractions in terms of membrane and bending with an arbitrary depth (*l*) from the notch root (a notched specimen analysed in [15]).

tion for the notch stress intensity solution procedures presented. The notched specimen used in [1-2] was shown in Fig. 6, where the detailed geometry is also given according to [1-2]. Note that in [1-2], detailed finite element analyses with very refine meshes were performed to generate stress distribution along the line from the notch root, as shown in Fig. 6. To avoid the influence of singular stresses at the notch root, a small radius was used at the notch root in [1-2]. For any crack size *a*, the corresponding crack face tractions in terms of p_m and p_b are given by the expressions in Eq. (8) and shown in Fig. 6, where a sharp notch is assumed, with the notch radius being zero. With Eq. (11), the stress intensity factor as a function of *a/t* can be analytically expressed for an arbitrarily short crack length (*a/t*), say, approaching zero. The corresponding stress intensity factor solutions are shown in Fig. 7 under both remote tension and bending conditions. The symbols are the weight-function based K solutions taken directly from [1-2]. A good agreement between the present solutions and those from [1-2] can be seen. For very small crack sizes (*a/t*), the present solutions using Eqs. (8) and (11) yield higher values than those given in [1-2]. This is mainly due to fact that they introduced a small radius at the notch root to void the stress singularity at the notch. In the present solution, the structural stress calculations are not affected by the presence of the sharp notch at the weld toe. If the notch stress effects are ignored, Eq. 9 produces the stress intensity factor solutions represented by the dashed lines in Fig. 7, which yields a reasonable prediction of K for *a/t* > 0.1 in both cases. Furthermore, the notch effects are seen to become dominant for *a/t* ≤ 0.1 or thereabout.

For elliptical cracks in the same notched geometry, again, the solutions developed by Glinka *et al.* [1-2] are used here for validation purposes. It is assumed the stress distribution from the 2D plane strain model applicable for the stress distributions in the thick plate (in the *z* direction) with the notch plane is orientated in x-y plane as shown in Fig. 6. The stress intensity factors based on weight function solutions at the deepest point for *a/c* = 0.25 and 1 (*c*: major axis of the elliptical crack) were taken from [1-2] for comparison purposes. The comparison between the solutions from [1-2] and the present procedures are summarised in Fig. 8. Again, since the stress solution used in [1] for integrating with the weight function was based on finite element calculation using a small radius at the notch root, the stress intensity factor as *a/t* approaching zero becomes lower than the present solutions, as expected.

3.4 Notch stress determination using t_1/t = 0.1

In the current notch stress intensity solutions, the notch stresses (self-equilibrating part of the stress state as depicted in Fig. 1 (c) are estimated by introducing a characteristic depth parameter t_1. In all calculations presented thus far, t_1/t =0.1 was used. As shown by Dong *et al.* [3, 6], the stress intensity solutions are not sensitive to the value of t_1/t, as long as adequate stress gradients are captured in Eq. (7) with respect to t_1. The selection of t_1/t = 0.1 can be established by the detailed observations of the stress intensity behaviour as crack size *a/t* becomes small. As shown in Fig. 9, the stress intensity factor solution based on Eq. (9) (without notch stress effects) exhibits incrementally slower increase as *a/t* varies from near 0 to *a/t* ~ 0.1, as seen in Fig. 9 (a). Such a trend can be more clearly shown if the derivative of *K* with respect to *a* (i.e., *dK/da*) is shown in Fig. 9 (b). In fact, as the crack size *a/t* becomes small, it can

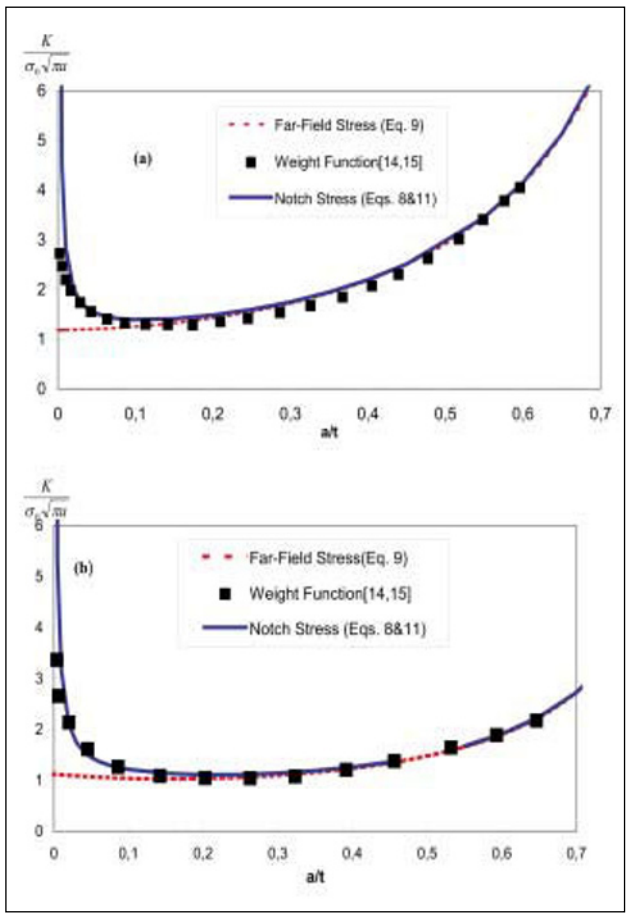

Fig. 7. Validations of the notch stress intensity solutions using published weight function results.
(a) Remote tension.
(b) Remote bending.

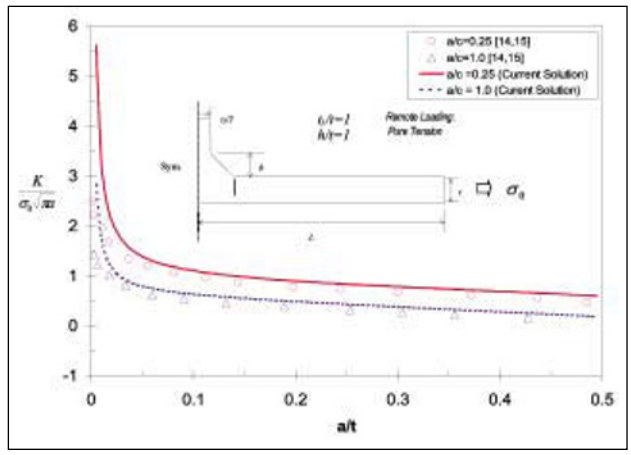

Fig. 8. Validation of current 3D elliptical crack K solutions in a notched plate using Eqs. (8) and (12).

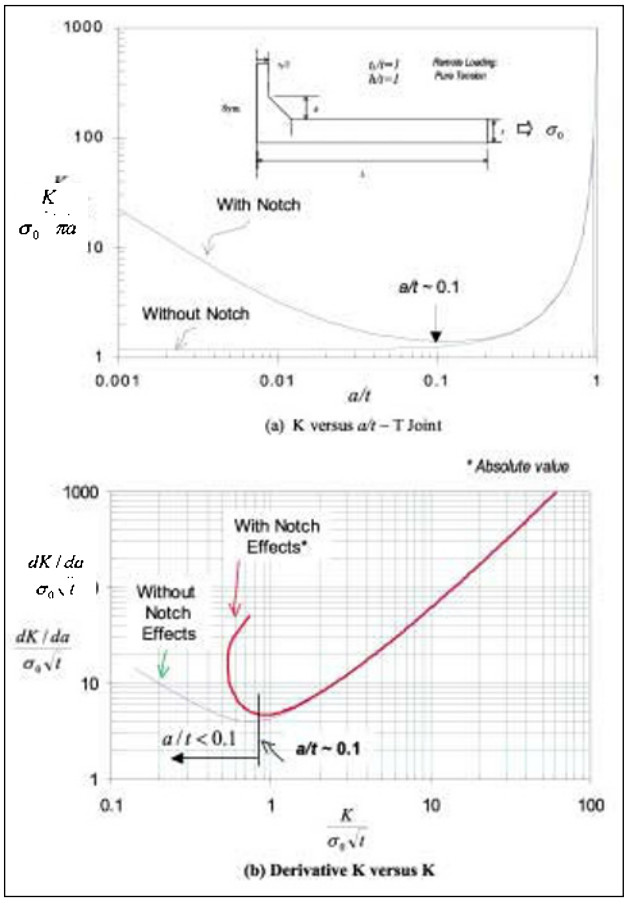

Fig. 9. Stress intensity changes as a function of crack size *a/t* for a notched specimen under remote tension.

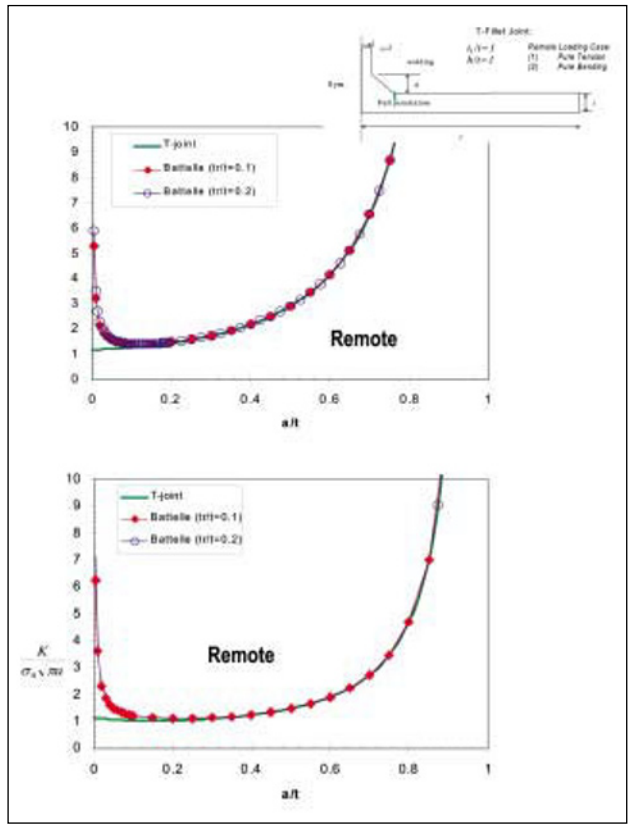

Fig. 10. Effects of t_1/t on stress intensity factor calculations for a T-joint.

be readily shown that $dK/da \sim 1/K$. As the notch effects are introduced, the stress intensity factor solutions are only affected within $a/t < 0.1$, as shown in Fig. 9, beyond which the stress intensity is governed by the through-thickness equivalent far-field stresses (σ_m^t, σ_b^t). Similar arguments can be made if remote loading is of bending type, as shown in Fig. 7 (b), or elliptical cracks shown in Fig. 8.

To further demonstrate the validity of the selection of $t_1/t = 0.1$, Fig. 10 shows the comparison of the K solutions between using $t_1/t = 0.1$ and $t_1/t = 0.2$. The difference in K solutions for the entire range of *a/t* under both remote tension and remote bending is not noticeable.

3.5 Stress intensity magnification factor M_k

Such notch-induced stress intensity behaviours can be more effectively demonstrated by defining a notch-induced stress intensity magnification factor as:

$$M_{kn} = \frac{K \text{ (with local notch effects)}}{K_n \text{ (based on through thickness } \sigma_m^t \text{ and } \sigma_b^t)} \quad (13)$$

In the above equation, K represents the total K due to both the far-field stress (e.g., Eq. 9) and the local notch stress effects (e.g., Eq. 11). The term K_n represents only the far-field stress contribution to the stress intensity factor as described by Eq. (9) for an edge crack or Eq. (10) for an elliptical crack, respectively. Note that the present definition of M_{kn} in Eq. (13), although resembling the so called M_k factor (see discussions in [11-12] in some of European codes and recommended practices for welded joints with sharp toe angle or notch, differs in that the denominator in Eq. (13) represents the through-thickness structural stress contributions, instead of nominal stresses. Any global stress concentration effects have already been taken into account in K_n. Therefore, M_{kn} reflects notch stress concentration effects captured by the self-equilibrating part of the actual stress state.

By examining a series of notched specimens in both 2D and 3D configurations, Fig. 11 summarises the M_{kn} computed as a function crack size *a/t* [6]. As shown in Fig. 10, M_{kn} approaches unity as crack size *a/t* approaches to, approximately, $a/t = 0.1$ in all cases. Such behaviour was also seen in M_k solutions reported in [5, 6] using crack tip elements for similar geometries. The differences between the edge crack solutions and elliptical solutions (at deepest position) are not significant in all cases. Consequently, $a/t \approx 0.1$ can be viewed as a characteristic depth beyond which the notch stress effects become negligible. In Fig. 6, the reference depth $t_1/t = 0.1$ is chosen to estimate the self-equilibrating notch stress distribution using the present stress analysis procedures.

3.6 Applications in notched fracture specimens

Fatigue crack growth rate data are mostly collected from some of the well-known notched fracture mechanics specimens, as shown in Fig. 12. The presence of a notch as a crack initiator often complicates the stress

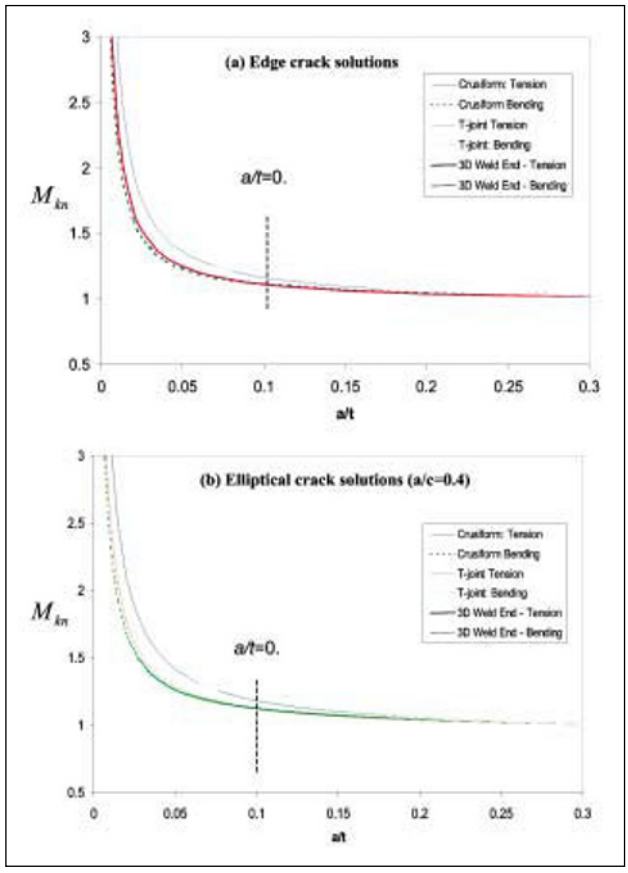

Fig. 11. Comparisons of stress intensity magnification factor M_{kn} at 135° sharp V notch [6] for various specimen geometries and loading conditions.
(a) Edge crack solutions using Eqs. (8) and (11).
(b) Elliptical crack solutions using Eqs. (8) and (12) for *a/c* = 0.4.

intensity factor calculations and often introduces a significant degree of inaccuracy when a crack is very small such as for $a/t < 0.1$, as recently demonstrated by Dong, *et al.* [3] in analyzing so called "anomalous short crack growth". By following the present notch stress solution procedures discussed earlier, both notch stresses (self-equilibrating) and equivalent far-field stress are calculated for each of the four specimens as discussed before. For stress intensity factor solutions, both CT and SEN specimens (Figs. 12 (a) and 12 (b)) with an edge crack are analysed using Eqs. (9) and (11) with both *a* and *t* defined in Fig. 12 to highlight the applications of the present structural stress and notch stress methods.

Notched CT and SEN specimens

For both CT and SEN specimens, the edge crack solutions given in Eqs. (9) and (11) are directly applicable after the far-field stresses (σ_m^t and σ_m^t) and (p_m, p_b, etc.) are calculated with respect to the ligament and crack definitions indicated in Fig. 12. An example of these is shown in Fig. 13 for the CT specimen with a key hole as a function of *a/t*. Such a specimen was used in [13] for crack growth rate testing. The solution marked with "without notch effects" is same as the typical handbook solution using nominal crack length combining the slot length with the key hole diameter in addition to *a* shown in the Figure. Note that the K solution indeed exhibits non-monotonic distribution when *a/t* is small. The same trend is also observed in notched SEN specimen used by Shin and Smith [14].

CN and DEN Specimens

The centre-notched (CN) specimens as shown in Fig. 12 (d) are demonstrated in detail in Fig. 14 (a) for demonstrating the present solution technique by considering the notch stress effects discussed earlier. The corresponding K solution has the following form:

$$K = p_s F_N F\sqrt{\pi a} \tag{15}$$

where the standard finite size correction F is directly taken from [9]:

$$F = \left\{1 - 0.025\left(\frac{R+a}{w}\right)^2 + 0.06\left(\frac{R+a}{w}\right)^4\right\}\cdot\sqrt{\sec\left(\frac{\pi(R+a)}{w}\right)}$$

The effects of the notch-stress induced gradient can be estimated by integrating p_m, p_b (Eq. (8)) over any given crack size a by adopting a simple weight function form corresponding to infinite body:

$$K = \frac{2}{\pi}\int_R^{R+a}\frac{p(x)dx}{\sqrt{a^2 - x^2}}$$

resulting:

$$F_N = \frac{2}{\pi}\sqrt{1+\frac{R}{a}}\cdot\left\{(1+\frac{2rR}{a})\cdot(\frac{\pi}{2} - \sin^{-1}(\frac{R}{a+R})) - \frac{2r}{a}\cdot\sqrt{(a+R)^2 - R^2}\right\}$$

Note in the above expression, $r = p_b / p_s$, as defined in Section 3. To calculate the stress intensity factor (K_n) due to the overall far-field stress (σ_m^t, σ_b^t), one simply needs to replace p_s, $\sigma(x)$, and r by:

$\sigma_s^t = \sigma_m^t + \sigma_b^t$, $\sigma(x) = \sigma_s^t - (2x/t)\,\sigma_b^t$, and $r = \sigma_b/\sigma_s$

in the above expressions. The corresponding K solutions are shown in Fig. 14. If the notch is treated as a part of the crack length, a handbook solution is also

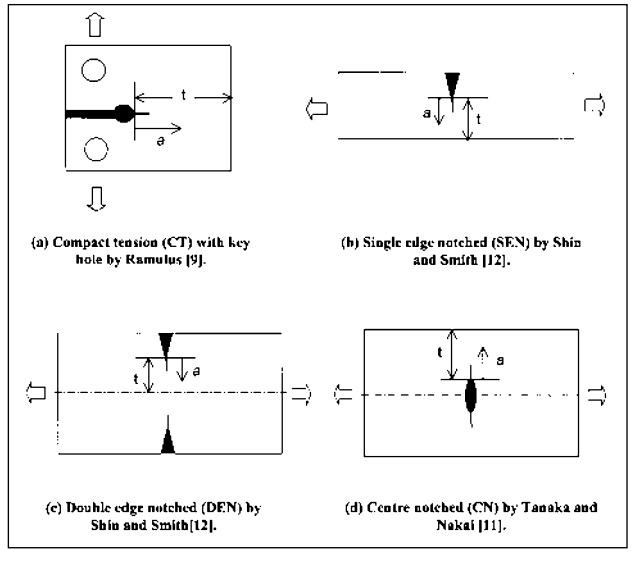

Fig. 12. Specimens used by various authors for characterising notch-induced short crack anomalous crack growth [9, 11, 12].
(Note that the definitions of ligament (t) and crack size (a) indicated are for using the notch stress intensity solutions presented in this paper).

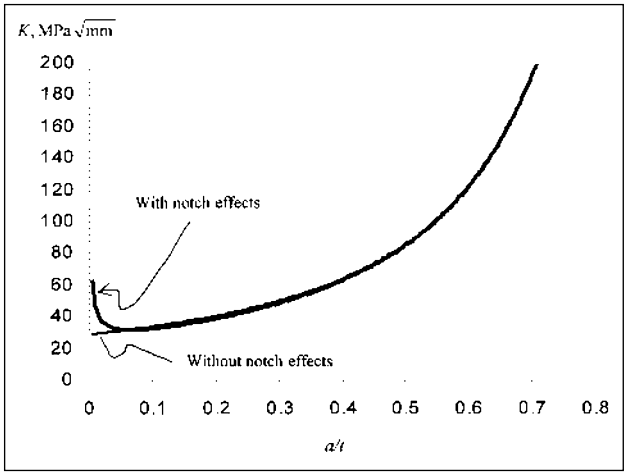

Fig. 13. Current notch stress based K solution for CT specimen withkey hole.
(a) CT specimen dimension used in [9].
(b) Comparison of the stress intensity solutions with and without considering notch effects under the given loading level given [9].

shown in Fig. 14 (b). It can be seen that the notch effects predicted by the present *K* solution procedures are only presented within about *a/t* < 0.1, consistent with observations for other notch geometries and specimen types discussed in earlier sections. The *K* solution for DEN specimens [15] can be estimated in a similar manner with the corresponding reference solutions from [9] and is not discussed here due to space limitation (see [3]).

4 CONCLUDING REMARKS

In this paper, a robust *K* estimation procedure is presented using a new mesh-insensitive structural stress procedure which directly provides the far-field stresses responsible for global equilibrium and self-equilibrating notch stresses estimated based on fracture mechanics principles. The present *K* solution procedure is particularly effective for fatigue and fracture evaluation of complex structures since relatively coarse mesh can be used as a typical structural mechanics calculation. Due to its analytical nature in the current notch stress estimation scheme, the crack size can be arbitrarily small. The validity of the current *K* solution procedure has been demonstrated by comparing existing *K* solutions obtained by weight function methods for welded joints. Furthermore, some well-known notched fracture mechanics specimens were also analysed to compare the present solutions with typical handbook solutions. The effectiveness of the current *K* solutions have been further demonstrated by its ability to correlate short crack growth data and the development of the master S-N curve approach for welded joints reported elsewhere.

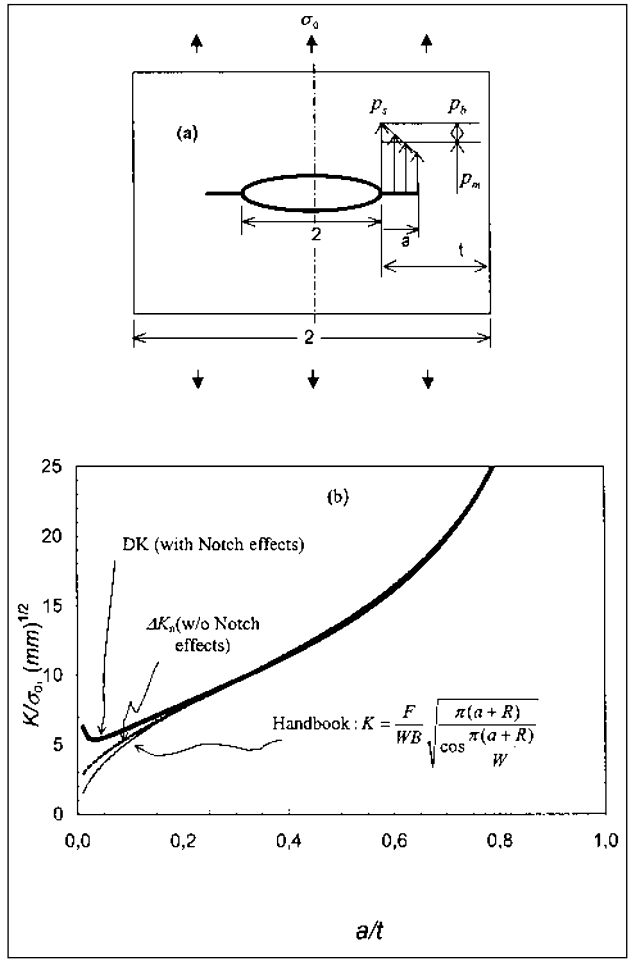

Fig. 14. Current stress intensity solutions for CN specimens.
(a) Definition of specimen and crack dimensions in CN specimen.
(b) Comparison of K solutions with and without notch effects.

REFERENCES

1. Niu X., Glinka G.: Stress intensity factor for semi-elliptical surface cracks in welded joints, International Journal of Fracture, 40, pp. 255-270, 1989.

2. Forbes J.W., Desjardins J.L., Glinka G., Burns, D.J.: Stress intensity factors for semi-elliptical surface cracks in weldments, 1991, OMAE – Volume III-B, Materials Engineering, ASME-1991, pp. 529-536.

3. Dong P., Hong J.K., Cao Z.: Stresses and stress intensities at notches: Anomalous crack growth, Revisited, International Journal of Fatigue, in press, 2003.

4. Dong P., Hong J.K., Cao Z.: A mesh-insensitive structural stress procedure for fatigue evaluation of welded structures, IIW doc. XIII-1902-01/XV-1089-01, July 2001.

5. Dong P.: "A structural stress definition and numerical implementation for fatigue analysis of welded joints", International Journal of Fatigue, 2001, vol. 23, pp. 865-876.

6. Dong P., Hong J.K., Osage D., Prager M.: Master S-N curve approach for welded components, Welding Research Council Bulletin, December 2002, No. 474.

7. Dong P., Hong J.K.: Analysis of hot spot stress and alternative structural stress methods, Proceedings of 22nd International OMAE Conference, June 8-13, 2003, Cancun, Mexico.

8. Zerbst U., Heerens J., Schwalbe K.H.: The fracture behavior of a welded tubular joint – an ESIS TC1.3 round-robin on failure assessment methods Part I: Experimental data base and brief summary of the results, Engineering Fracture Mechanics, 2002, vol. 69, pp. 1093-1100.

9. Tada H., Paris P.C., Irwin G.R.: The stress analysis of cracks handbook, third edition, ASME, 2000.

10. Shiratori M., Niyoshi T., Tanikawa K.: Analysis of stress intensity factors for surface cracks subjected to arbitrarily distributed surface stress, Stress Intensity Factor Handbook, Y. Murakami *et al.* Eds, Pergamon, 1987, vol. 2, pp. 698-705.

11. Hobbacher A.: Stress intensity factors of welded joints, Engineering Fracture Mechanics, 1993, vol. 46, No. 2, pp. 173-182.

12. Maddox S.J.: Assessing the significance of flaws in welds subjected to fatigue, Welding Journal Research Supplement, 1974, pp. 401s-409s.

13. Ramulu M.: Experimental investigation of subcritical growth of a surface flaw, Surface crack crack growth: models, experiments, and structures, ASTM STP 1060, W.G. Reuter, J.H. Underwood, and J.C. Newman, Jr. Eds., 1990, pp. 333-347.

14. Shin C.S., Smith R.A.: Fatigue crack growth at stress concentrations- the role of notch plasticity and crack closure, Engineering Facture Mechanics, 1988, vol. 29, No. 3, pp. 301-315.

15. Tanaka K., Nakai Y.: Propagation and non-propagation of short fatigue cracks at a sharp notch, Fatigue of Engineering Materials and Structures, 1983, vol. 6, No. 4, pp. 315-327.